Publishing House
AKAPIT

COMPUTER METHODS IN MATERIALS SCIENCE

Informatyka w Technologii Materiałów

Vol. 9, 2009, No. 4

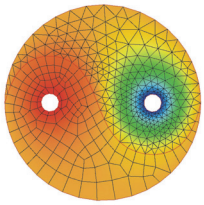

THERMAL MODELING OF FRICTION STIR WELDING OF Sc-MODIFIED Al-Zn-Mg-Cu ALLOY

CARTER HAMILTON[1]*, STANISŁAW DYMEK[2], OLEG SENKOV[3]

[1]Department of Mechanical and Manufacturing Engineering
Miami University, Oxford, OH
[2]Faculty of Metals Engineering and Industrial Computer Science
AGH University of Science and Technology, Kraków, Poland
[3]UES, Inc., 4401 Dayton-Xenia Rd., Dayton, OH 45432-1894, USA
**Corresponding Author: hamiltbc@muohio.edu*

Abstract

Small additions of scandium to Al-Zn-Mg-Cu 7000 series alloys can significantly improve mechanical properties and augment the strength retention at low and elevated temperatures. This research program evaluates the residual properties of Sc-modified Al-Zn-Mg-Cu alloy extrusions joined through friction stir welding (FSW). Mechanical testing was performed on the baseline material and on panels friction stir welded at 175, 225, 250, 300, 350 and 400 RPM (all other weld parameters were held constant). A thermal model of friction stir welding was developed utilizing an energy-based scaling factor to account for tool slip. The proposed slip factor is derived from an empirical relationship between the ratio of the maximum welding temperature to the solidus temperature and energy per unit length of weld. The thermal model successfully predicts the maximum welding temperatures over a range of energy levels, and the mechanical behavior is correlated to the temperature distribution predicted by the model.

Key words: friction stir welding, aluminum, scandium, mechanical properties

1. INTRODUCTION

As the aerospace industry produces new and more efficient airframes, the need to provide high-strength, lightweight alloys that meet the aggressive design objectives for mechanical performance, manufacturability and service life arises. Conventional Al-Zn-Mg-Cu 7000 series alloys are widely used in aerospace applications due to their favorable mechanical properties. However, these properties degrade above 150°C due to the coarsening and/or dissolution of the strengthening phases within the microstructure. Additions of scandium (Sc) and zirconium (Zr) to 7000 series alloys can stabilize the microstructure at these elevated temperatures and can augment the mechanical performance through the formation of fine, secondary strengthening phases such as Al_3(Sc, Zr) (Senkova et al., 2006; Bhat et al., 2005). Because the nanometer-sized Al_3(Sc, Zr) particles also stabilize the microstructure formed during hot working operations and inhibit recrystallization during heat treatment, the potential for enhanced residual properties following joining operations, such as friction stir welding (FSW), arises.

Friction stir welded joints display excellent mechanical properties when compared to conventional fusion welds, and as such, the aerospace industry is embracing FSW technology and implementing new welding capabilities into their manufacturing sectors

ISSN 1641-8581

(Thomas, 1991; Dawes & Thomas, 1995; Sutton et al., 2004, Dracup & Arbegast, 1999; von Strombeck et al., 1999, Hamilton et al., 2007). Since no melting occurs during FSW, the process is performed at much lower temperatures than conventional welding techniques and circumvents many of the environmental and safety issues associated with these other welding methods. The plastic deformation and temperature profile during FSW produce a microstructure characterized by a central weld nugget surrounded by a thermo-mechanically affected zone (TMAZ) and heat-affected zone (HAZ). Since its introduction, numerous researchers have sought to characterize the principles of FSW and to model the microstructural evolution and temperature behavior.

Despite the complex flow of material during FSW, researchers have found success in modeling the heat transfer characteristics of FSW. For example, Frigaard et al. (2001) developed a finite difference thermal model for a moving heat source and correlated the predicted temperature profile with the measured temperature profile for friction stir welded AA6082-T6 and AA7108-T79 extrusions. Utilizing a three-dimensional visco-plastic model, Ulysse (2002) studied the impact of varying weld parameters on the temperature distribution in AA7050-T7451 plate. Khandkar et al. (2006) introduced a model of heat input based on the torque of the FSW tool that they then successfully utilized to model the temperature history of friction stir welded AA6061-T651 plate. Early thermal models, such as that of Colegrove and Shercliff (2005), however, did not account for the slip that occurs as the welding temperature approaches the solidus temperature of the alloy which results in a softening of the tool/workpiece interface. As a result, these models significantly over predicted the maximum temperature for "hot" welding conditions. The current status of FSW research has been well summarized by Mishra and Ma (2005). The following research program characterizes the mechanical behavior of developmental, Sc-modified Al-Zn-Mg-Cu extrusions (SSA038-T6) joined by friction stir welding.

The chemical composition of SSA038 is summarized in table 1 along with that of aluminum 7075 for reference and comparison (Senkova et al., 2006). Whereas 7075 primarily utilizes chromium to control grain growth and recrystallization, SSA038 utilizes the synergistic combination of scandium and zirconium to stabilize the microstructure. Also the SSA038 chemistry has a higher level of zinc than 7075. The zinc level of SSA038 is more akin to that of the 7050 or 7136 alloys.

Table 1. *Chemical Composition of SSA038 with 7075 as Reference*

Element	Weight Percent	
	SSA038	7075
Zn	7.11	5.60
Mg	2.14	2.50
Cu	1.56	1.60
Mn	0.25	0.30
Zr	0.17	< 0.05
Sc	0.38	--
Cr	< 0.05	0.23
Ti	< 0.05	0.20
Other, Each	0.35	1.03
Al	Balance	

2. EXPERIMENTAL PROCEDURE

2.1. Friction Stir Welding

For this investigation, SSA038 billets were produced by UES, Inc. through direct chill casting and then extruded as 50.4 mm x 6.35 mm bars. Following extrusion, the bars were heat treated to a –T6 temper through the following schedule: (1) solution heat treat at 460°C for one hour followed by an additional hour at 480°C, (2) rapid quench in water to room temperature and (3) age at 120°C for 19 hours. After heat treatment, the bars were cut into twelve, 305 mm lengths and sent to the Edison Welding Institute to produce six friction stir welds in the configuration represented in figure 1. As shown in the diagram, FSW occurs along the L-direction of the extrusions with a clockwise tool rotation. The diameter of the FSW tool shoulder was 17.8 mm, the pin diameter tapered linearly from 10.3 mm at the tool shoulder to 7.7 mm at the tip and the pin depth was 6.1 mm. With a constant weld velocity of 2.1 mm/s and a constant applied force of 22 kN, unique welds were produced at the following tool rotation speeds: 175, 225, 250, 300, 350 and 400 RPM.

Utilizing a Mikron M7815 Thermal Imaging Camera during welding, the temperature profile across the weld was experimentally recorded for each condition. The thermal emissivity for the infrared data was calibrated by imaging an extrusion length heated to 460°C and adjusting the emissivity value until the recorded temperature of the camera matched the reference temperature. The appropriate

thermal emissivity value was determined to be 0.285. The experimental temperature data were used to verify the efficacy of the computer thermal model developed during this investigation.

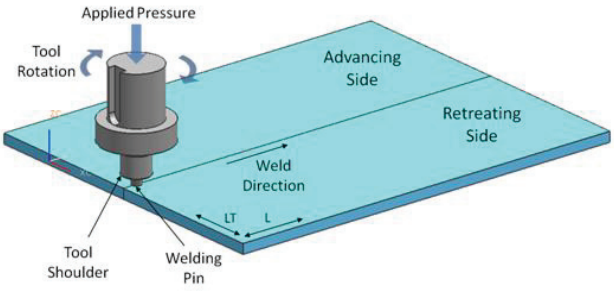

Fig. 1. *Schematic of Butt-Weld Geometry and FSW Orientation*

2.2. Mechanical Testing

Subsequent to joining, the welded panels were stored at room temperature and allowed to naturally age for at least 30 days prior to testing and investigation. From the welded panels of each tool rotation speed, full thickness (6.35 mm) tensile samples were excised perpendicular to the friction stir weld with the weld centered along the tensile specimen in the reduced section as shown in figure 2. In this orientation, the load is applied transverse to the weld direction and across all microstructural regions associated with the welding process, i.e., weld nugget, HAZ and TMAZ. In addition to the welded tensile specimens, tensile bars of the same geometry and dimensions were also excised from an area well away from the weld region for baseline property comparison. All tensile tests were performed in accordance with ASTM E 8 utilizing an Instron 5867 screw driven test frame with a 30 kN load cell and a 0.001 – 500 mm/min speed range. Specimen extension, crosshead deflection and load were recorded throughout the test duration. Specimen extension was measured by means of an extensometer attached to the reduced section that spanned the width of the weld. The yield strength, σ_y, was obtained by the 0.2% offset method, and the elastic modulus was determined by fitting a linear regression to the elastic region of the stress-strain curve. Elongation, e, was determined by scribing marks with known separation within the reduced section prior to testing and measuring their separation after testing.

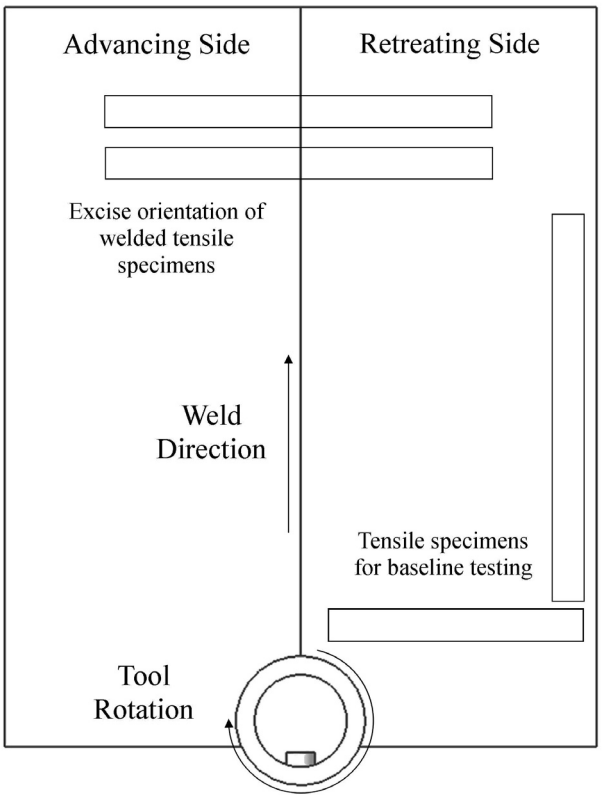

Fig. 2. *Excise Location of Tensile Specimens and Corrosion Coupons from FSW Panels*

3. RESULTS AND DISCUSSION

3.1. Mechanical Properties

Six different tool rotation speeds were examined to assess the impact of changing weld parameters on the residual properties and to identify the optimum weld condition leading to the highest joint efficiency. Since the weld velocity and the applied force were held constant during FSW and only the tool rotation speed was varied, the tool RPM provides a relative measure of the energy imparted to the aluminum extrusions due to changes in the process parameters. It is, however, more appropriate to evaluate the influence of the process parameters, weld velocity (v_w), tool rotation speed (ω) and applied force (F), during friction stir welding in terms of the total heat or energy imparted to the workpieces during welding, rather than the impact of a single parameter. Since varying any of the identified parameters changes the heat input of the system, correlating the heat input with the resultant material behavior gives greater insight into the friction stir welding process.

For this reason, Khandkar et al.'s (2003) torque-based model was used to determine the energy input per unit length of weld for the Sc-modified Al-Zn-Mg-Cu alloy extrusions and to correlate this quantity

with the observed material properties at various tool rotation speeds. The total torque, T_{total}, can be expressed as the sum of torque contributions from the tool shoulder against the workpiece, the bottom of the tool pin against thickness material and the pin surface against thickness material. Introducing τ as the shear stress during welding, assumed to be uniform across all tool-workpiece interfaces, the total torque then becomes:

$$T_{total} = \int_{r_{i1}}^{r_o} (\tau r)(2\pi r)dr + \int_{0}^{r_{i2}} (\tau r)(2\pi r)dr + 2\pi\tau r_i^2 h \quad (1)$$

where r_o is the radius of the tool shoulder, r_{i1} is the radius of the pin at the tool shoulder, r_{i2} is the radius of the pin at the pin bottom and h is the pin height. In actuality, the magnitude of the shear stress will vary with the local welding temperature. However, for simplification, the temperature dependence is ignored, and the shear stress is estimated from the applied force during FSW. To further simplify the evaluation of equation 1, the taper of the welding pin is ignored, i.e., $r_{i1} = r_{i2}$, thus

$$T_{total} = \tau(\frac{2}{3}\pi r_o^3 + 2\pi r_i^2 h) = 2\mu F(\frac{r_o}{3} + \frac{r_i^2}{r_o^2} h) \quad (2)$$

where F is the applied force and μ is the coefficient of friction between the tool and the extrusions. The energy per unit length of weld, E_l, is found by dividing the average power, P_{avg}, by the weld velocity to yield the expression in equation 3:

$$E_l = \frac{P_{avg}}{v_w} = T_{total}\frac{\omega}{v_w} \quad (3)$$

Though the applied force during FSW was set to 22 kN, real time data from the welding trials revealed that the load oscillated as the machine continuously corrected the load toward the set point. Consequently, the average load during welding deviated from the desired set point. Therefore, the average load was determined from the recorded data for each weld condition and was utilized in the analysis of that condition. The recorded data verified that the weld velocity remained constant at 2.1 mm/s for all welding trials. Using a coefficient of sliding friction between aluminum and mild steel of 0.5 (Frigaard et al., 2001; Soundararajan et al., 2005), the E_l were determined for each tool rotation speed.

Table 2 summarizes the E_l values and the average mechanical properties of weld joints for different FSW conditions. The joint efficiency is defined as the ratio of the tensile strength for a given weld condition to the L-direction baseline tensile strength. After FSW at 175 RPM, the yield strength (YS), ultimate tensile strength (UTS), and elongation (e) decreased relative to the baseline properties. This decrease can be associated with overaging and/or annealing due to FSW-induced heating. Increasing from 175 RPM to 250 RPM did not affect YS. However, e increased to 10% and UTS increased to 451 MPa. Increasing the rotation speed from 250 RPM to 350 RPM decreased the YS, UTS, and e to 294 MPa, 381 MPa and 5.7%, respectively. The correlation between e and UTS between 175 to 350 RPM is noteworthy. That is, as the weld joint ductility increases, the UTS and joint efficiency simultaneously increase. As a result, the FSW parameters that promote superior joint ductility also lead to higher UTS. A rise from 350 RPM to 400 RPM slightly increased YS (to 306 MPa), but considerably decreased e (to 3.0%) with little impact on the UTS.

Table 2. *Summary of Mechanical Properties for Each Weld Condition*

Rotation Speed (RPM)	E_l (J/mm)	UTS σ_{TS} (MPa)	YS σ_y (MPa)	*EL e* (%)	Joint Eff. (%)
Baseline (L)	--	663	605	12.0	--
Baseline (LT)	--	651	597	15.4	--
175	842	406	338	5.7	61
225	938	443	337	7.2	67
250	977	451	337	10.0	68
300	1331	446	309	7.9	67
350	1502	381	294	5.7	57
400	1567	383	306	3.0	58

Figure 3 displays the relationship between the strength properties and the energy per unit length of weld, and clearly shows the local maximum that is realized at 250 RPM (~980 J/mm). An analysis of variance reveals that both correlations between the tensile strength and yield strength with the applied weld energy are statistically significant.

As the welding energy increases, the welding temperatures of the workpieces also increase. The SSA038 alloy is a precipitation strengthened aluminum alloy, and its strength in the –T6 temper is controlled by *GPII* zones and η' particles, as well as by $Al_3(Sc,Zr)$ nano-dispersoids (Senkov et al., 2008a; Senkov et al., 2008b). A considerable decrease in both YS and UTS after welding is a strong indication that the welding temperature was significantly

higher than the aging temperature (120ºC), promoting: (a) the dissolution of *GPII* zones, (b) coarsening of η' particles and their transformation to equilibrium η, i.e overaging, and/or (c) the partial dissolution of η' and η followed by re-precipitation after cooling. To understand the trend in mechanical behavior observed in figure 3, a thermal model of friction stir welding was developed using NX 5.0.

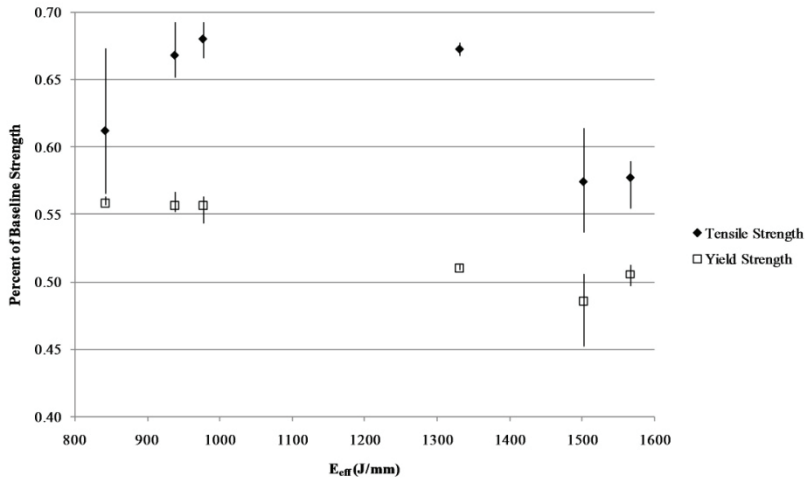

Fig. 3. *Ultimate and Yield Strengths as a function of the Energy per Unit Length of Weld (one standard deviation shown)*

3.2. Thermal Modeling

For the FSW representation and tool coordinate system shown in figure 4, the governing heat equation for a moving heat source is given by (Nandan et al., 2007):

$$\rho c_p \nabla(uT) = -\rho c_p v_x \frac{\partial T}{\partial x} + \nabla(k\nabla T) + S_i + S_b \qquad (4)$$

where u is the plastic flow velocity, v_x is the welding velocity in the x-direction, S_i is the source term for the heat generation due to the tool/workpiece interface, S_b is the source term for the heat generation rate due to plastic deformation away from the interface, and all other terms have their previous meaning. The heat flux, q, at the tool/workpiece interface may be derived from the S_i term and is given by the following expression:

$$q = \delta \mu P_N \omega r \qquad (5)$$

where δ is the slip factor, P_N is the normal pressure relative to a tool face, μ is the coefficient of friction between the tool and workpiece and r is the radial distance from the tool center axis as shown in figure 4.

In an earlier work, Hamilton et al. (2008) proposed that a characteristic relationship exists for aluminum alloys during friction stir welding between the ratio of the maximum weld temperature to the solidus temperature of the alloy, T_{max}/T_s, and the energy per unit length of weld, E_l. From that relationship, the following energy-dependent expression for the slip factor was then derived:

$$\delta_E = \exp\left(-\frac{E_l}{(E_l)_{\max}}\right) \qquad (6)$$

where $(E_l)_{max}$, the maximum effective energy, is defined as the energy level for which the maximum welding temperature is equal to the solidus temperature of the alloy (i.e., $T_{max}/T_s = 1$). The solidus temperature for SSA038 is 528°C. In equation 6, δ_E effectively represents the efficiency of frictional heat transfer, such that, when $\delta_E = 1$, sticky friction dominates. As E_l increases, the tool/workpiece interface softens, and the extent of slip increases, lowering the effectiveness of the heat transfer process. At the limit of $E_l = (E_l)_{max}$, $\delta_E = 0.37$.

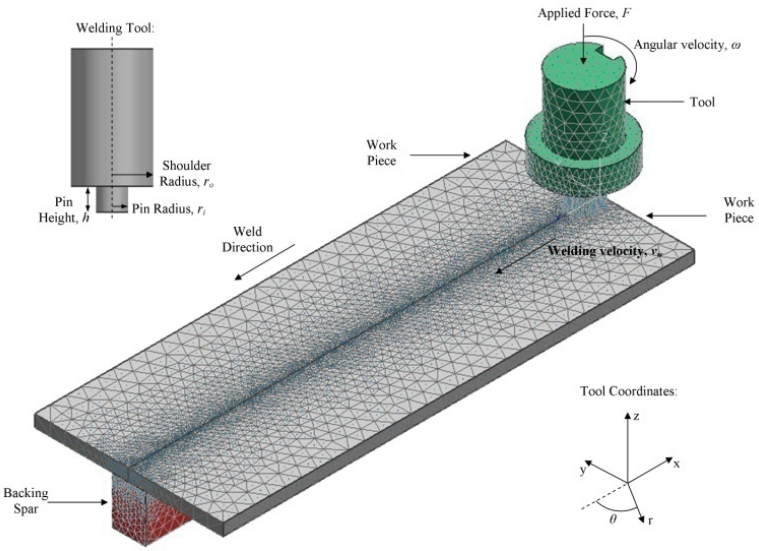

Fig. 4. *Finite Element Model of FSW, Tool Coordinate System and Tool Geometry*

For the tool shoulder and pin bottom, the normal pressure, P_N, is the applied pressure on the workpiece during welding. For the interface between the side of the pin and the workpiece, however, the normal pressure is the pressure that resists the tool as it traverses the workpiece during welding. For typical welding conditions, this pressure is significantly less than the applied pressure. Therefore, the frictional heat flux is primarily generated by the pin bottom and tool shoulder, and the heat flux at the pin side/workpiece interface is set equal to zero. The thermal model utilizes the average heat flux on the pin bottom, $q_{pinbottom}$, and tool shoulder, $q_{shoulder}$, to calculate the maximum welding temperatures. Assuming axisymmetric heat generation, these heat flux equations given in equations 7 and 8 are:

$$q_{pinbottom} = \frac{\int_0^{r_i} \delta_E \mu P_N \omega r dr}{r_i} = \frac{\delta_E \mu P_N \omega r_i}{2} \tag{7}$$

and

$$q_{shoulder} = \frac{\int_{r_i}^{r_o} \delta_E \mu P_N \omega r dr}{r_o - r_i} = \frac{\delta_E \mu P_N \omega (r_o^2 - r_i^2)}{2(r_o - r_i)} \tag{8}$$

where all terms have their previous meaning.

Figure 4 shows the three-dimensional, finite element model of FSW. This approach focuses on the temperature distribution produced during the joining process, but does not address mechanical interactions between the tool and workpiece. A backing spar, as opposed to a full backing plate, was chosen to reduce the number of equations to be solved and to shorten the computer processing time while still capturing the heat transfer characteristics between the workpiece and backing plate. The width of the backing spar is equal to the diameter of the tool, and the height is 25.4 mm. The model assumes that perfect contact exists between the two workpieces along the weld line and between the tool shoulder and the workpieces. A gap thermal conductivity of 157 *W/mK*, equal to the thermal conductivity of SSA038, was applied between the pin bottom and the bottom of workpieces. For the boundaries exposed to ambient conditions, the convective coefficient was set to 15 W/m^2K. The remaining boundary conditions and thermal couplings were determined using the thermal images recorded during welding. For the tool top and spar bottom, a convection coefficient of 200 W/m^2K was applied, and for the area outside of and adjacent to the backing spar, a convective coefficient of 100 W/m^2K was used to represent the dissipation of heat into the backing plate. Lastly, a heat transfer coefficient of 250 W/m^2K was chosen to define the conductance of heat between the bottom of the workpieces and the backing spar. In this model, heat dissipation due to radiation was ignored.

Figure 5 plots the experimental temperature profile of the 400 RPM condition with the profile predicted by the thermal model for the same location. The profile extends from the weld line into the workpiece along the top surface of the FSW configuration. Although the model slightly under predicts the temperatures, the predicted profile shows good agreement with the magnitude and shape of the experimental data.

With the heat fluxes determined from equations 7 and 8, the thermal model was then used to determine the maximum welding temperatures of SSA038-T6 for the six, unique energy levels investigated. Table 3 summarizes these temperatures. As predicted for each weld condition, the maximum welding temperature is considerably higher than the aging temperature of the alloy (120ºC). This over-heat explains the decrease in the tensile strength of the welded material relative to the –T6 baseline condition.

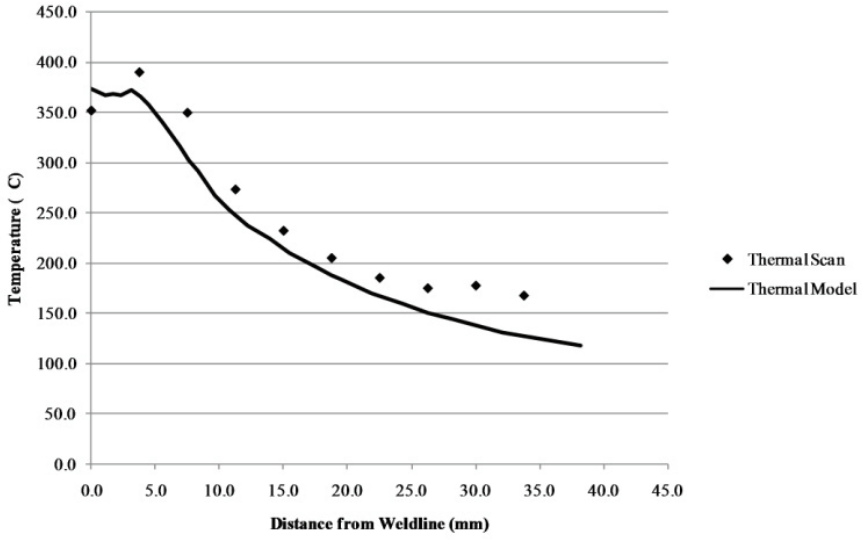

Fig. 5. *Experimental Temperature Profile Compared to Temperature Profile Predicted by the Thermal Model*

Table 3. *Predicted Maximum Welding Temperatures for each Weld Condition*

Rotation Speed (RPM)	E_l (J/mm)	Predicted Max. Temp. (°C)
175	842	264
225	938	282
250	977	289
300	1331	342
350	1502	362
400	1567	386

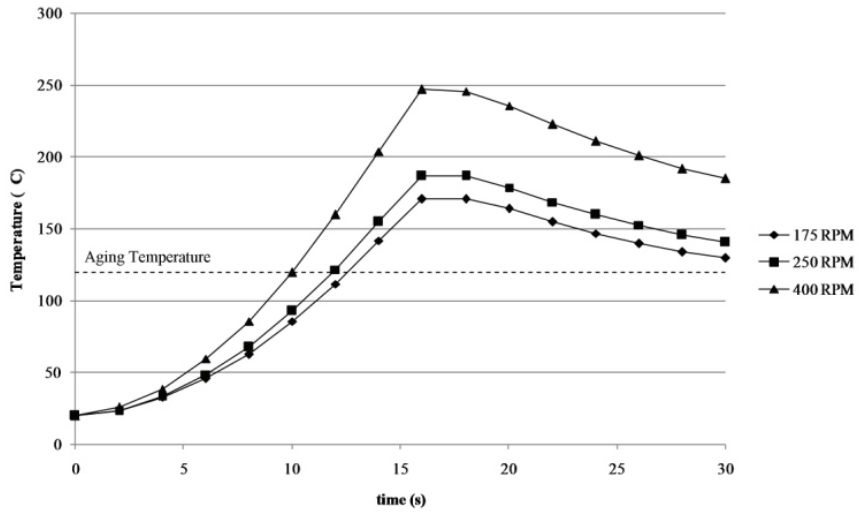

Fig. 6. *Transient Temperature Profiles for a Top Surface Node at the Interface Between the Weld and HAZ*

Figure 6 shows the transient temperature profiles that were experimentally determined for a node located on the top surface of the workpiece at the interface between the weld and HAZ. Welding conditions at 175 and 250 RPM reveal similar dwell times above the aging temperature and maximum temperatures that are only 16°C different in magnitude. On the other hand, welding at 400 RPM shows a longer dwell time above the aging temperature, and a maximum temperature that is 50°C greater than that observed at 250 RPM. The similar temperature history between welds produced at 175, 225 and 250 RPM explains the similar values of the yield strength. The decrease in YS of the welds relative to the YS of the –T6 baseline condition is most likely due to overaging, i.e., dissolution of the *GPII* zones, coarsening of η' particles and formation and growth of equilibrium η (Senkov et al., 2008a; Senkov et al., 2008b). Between 175 and 250 RPM, the strain hardening that occurs after yielding provides higher UTS at larger plastic strains (Argon, 2008), and the improved ductility within this range may simply be due to a superior weld quality produced at higher rotation speeds. This explanation, however, must be verified by microstructural examination.

Between the predicted maximum welding temperatures of 342ºC and 386ºC for 300 and 400 RPM, all metastable particles dissolve and only coarse equilibrium η phase particles and $Al_3(Sc,Zr)$ nanodispersoids are present within the FCC Al matrix of SSA038 (Senkova et al., 2006). As a result, the yield strength values approach the YS value of the annealed alloy (~273 MPa) (Senkova et al., 2006). The slightly higher YS after 400 RPM than after 350 RPM can be due to higher super-saturation of the alloying elements after heating to a higher temperature, resulting in the re-precipitation of a larger amount of metastable particles upon cooling.

Similar to the welding conditions at the lower rotation speeds, the UTS values are likely controlled by the plastic strain achieved after yielding and before fracture, so that the UTS decreases with a decrease in the plastic strain (ductility). The latter is probably controlled by the weld quality, and as such, the weld parameters corresponding to 250 RPM produce the highest weld quality, and, therefore, correspond to the optimum welding condition.

4. CONCLUSIONS

Al-Zn-Mg-Cu aluminum extrusions modified with scandium were friction stir welded in a butt-weld configuration at six different tool rotation speeds (i.e., 175, 225, 250, 300, 350 and 400 RPM) and evaluated for residual properties. Mechanical testing revealed the highest joint efficiency at 250 RPM, corresponding to an energy per unit length of weld of 1000 J/mm. The tensile strength falls off sharply when the welding energies surpass 1300 J/mm. The trend in mechanical properties may be due to the competition between secondary nucleation of strengthening phases that dominates at weld energies below 1300 J/mm and precipitate coarsening that dominates at energies above 1300 J/mm. A thermal model of FSW quantifies the welding temperatures above the aging temperatures of SSA038 and the dwell times above this temperature.

ACKNOWLEDGEMENTS

The authors acknowledge the Polish Ministry of Science and Higher Education (Grant No. N 507 094 32/2648), UES, Inc. (Dayton, Ohio USA) and the Materials and Manufacturing Directorate at Wright-Patterson AFB (Dayton, Ohio USA) for their support of this research.

REFERENCES

Argon, A.S., 2008, *Strengthening Mechanisms in Crystal Plasticity*, Oxford University Press, Oxford.

Bhat, R. B., Schloz, J. D., Senkova, S. V., Senkov, O. N., 2005, Microstructure and Properties of Cast Ingots of Al-Zn-Mg-Cu Alloys Modified with Sc and Zr, *Metall. Mater. Trans. A*, 36 (8), 2115–2126.

Dawes, C., Thomas, W., 1995, TWI Bulletin 6, November/December, 124.

Dracup, B. J., Arbegast, W. J., 1999, Friction Stir Welding as a Rivet Replacement Technology, *Proceedings of the 1999 SAE Aerospace Automated Fastening Conference & Exposition*, Memphis, TN, October 5-7.

Frigaard, O., Grong, O., Midling, O. T., 2001, A Process Model for Friction Stir Welding of Age Hardening Aluminum Alloys, *Metall. Mater. Trans. A*, 32 (5), 1189-1200.

Hamilton, C., Dymek, S., Blicharski, M., 2007, Comparison Of Mechanical Properties For 6101-T6 Extrusions Welded By Friction Stir Welding And Metal Inert Gas Welding, *Arch. Metall. Mater.*, 52, 67-72.

Hamilton, C., Dymek, S., Sommers, A., 2008, A Thermal Model of Friction Stir Welding in Aluminum Alloys, *Int. J. Mach. Tool. Manu.*, 48, 1120–1130.

Khandkar, M.Z.H., Khan, J.A., Reynolds, A.P., 2003, Prediction of Temperature Distribution and Thermal History during Friction Stir Welding: Input Torque Based Model, *Sci. Technol. Weld. Join.*, 8 (3), 165-174.

Khandkar, M.Z.H., Khan, J.A., Reynolds, A.P., Sutton, M.A., 2006, Predicting Residual Thermal Stresses in Friction Stir Welded Metals, *J. Mater. Process. Tech.*, 174, 195-203.

Mishra, R.S., Ma, Z.Y., 2005, Friction Stir Welding and Processing, *Mater. Sci. Eng. R*, 50, 3-78.

Nandan, R., Roy, G.G., Lienert, T.J., Debroy, T., 2007, Three-dimensional Heat and Material Flow during Friction Stir Welding of Mild Steel, *Acta Mater.*, 55, 883-895.

Senkov, O.N., Shagiev, M.R., Senkova, S.V., 2008a, Effect of Sc on Aging Kinetics in a Direct Chill Cast Al-Zn-Mg-Cu Alloy, *Metall. Mater. Trans. A*, 39, 1034-1053.

Senkov, O.N., Shaghiev, M.R., Senkova, S.V., Miracle, D.B., 2008b, Precipitation of $Al_3(Sc,Zr)$ Particles in a Direct Chill Cast Al-Zn-Mg-Cu-Sc-Zr Alloy during Conventional Solution Heat Treatment and Its Effect on Tensile Properties, *Acta Mater.*, 56 (15), 3723-3738.

Senkova, S.V., Senkov, O.N., Miracle, D.B., 2006, Cryogenic and Elevated Temperature Strengths of an Al-Zn-Mg-Cu Alloy Modified with Sc and Zr, *Metall. Mater. Trans. A*, 57 (12), 3569-3575.

Soundararajan, V., Zekovic, S., Kovacevic. R., 2005, Thermo-mechanical Model with Adaptive Boundary Conditions for Friction Stir Welding of Al AA6061, *Int. J. Mach. Tool. Manu.*, 45, 1577-1587.

Sutton, M.A., Yang, B.C., Reynolds, A.P., Yan, J.H., 2004, Banded Microstructure in 2024-T351 and 2524-T351 Aluminum Friction Stir Welds–Part II. Mechanical Characterization, *Mater. Sci. Eng. A*, 364, 66-74.

Thomas, W.M. et al., 1991, Great Britain Patent Application No. 9125978.8 (December).

Ulysse, P., 2002, Three-Dimensional Modeling of the Friction Stir-Welding Process, *Int. J. Mach. Tool. Manu.,* 42, 1549-1557.

von Strombeck, A., dos Santos, J.F., Torster, F., Laureano, P., Kocak, M., 1999, Fracture Toughness of FSW Joints on Aluminum Alloys, *Proceedings of the First International Symposium on Friction Stir Welding*, Thousand Oaks, CA, USA, June 14-16.

MODEL CIEPLNY PROCESU ŁĄCZENIA TARCIOWEGO Z MIESZANIEM MATERIAŁU ZGRZEINY NA PRZYKŁADZIE STOPU Al-Zn-Mg-Cu MODYFIKOWANEGO SKANDEM

Streszczenie

Niewielki dodatek skandu do stopu Al-Zn-Mg-Cu z serii 7000 może w znaczący sposób poprawić właściwości mechaniczne w temperaturze pokojowej oraz powstrzymać spadek wytrzymałości w temperaturze podwyższonej. W zaprezentowanych badaniach dokonano oceny właściwości mechanicznych połączeń stopu Al-Zn-Mg-Cu modyfikowanego skandem wykonanych metodą zgrzewania tarciowego z mieszaniem materialu zgrzeiny (FSW). Badania mechaniczne wykonano na materiale rodzimym oraz na próbkach zgrzewanych z prędkościami obrotowymi narzędzia 175, 225, 250, 300, 350 i 400 obrotów na minutę (przy jednakowych pozostałych parametrach procesu). Opracowano komputerowy model cieplny zgrzewania tarciowego z mieszaniem materiału zgrzeiny wykorzystujący energetyczny współczynnik ujmujący poślizg narzędzia w trakcie procesu. Współczynnik ten zaproponowano w oparciu o doświadczalną zależność pomiędzy stosunkiem maksymalnej temperatury podczas zgrzewania do temperatury solidus oraz energii wydatkowanej na jednostkę długości zgrzeiny. Opracowany model bardzo dobrze przewiduje maksymalne temperatury zgrzewania dla szerokiego zakresu energii oraz wykazuje dobrą korelację właściwości mechanicznych z temperaturą przewidzianą przez model.

Received: April 2, 2009
Received in a revised form: May 13, 2009
Accepted: May 15, 2009